Journal of Materials Science & Technology 57 (2020) 146–152

Contents lists available at ScienceDirect

Journal of Materials Science & Technology

journal homepage: www.jmst.org

Research Article

Mitigating microbiologically influenced corrosion of an oilfield biofilm consortium on carbon steel in enriched hydrotest fluid using 2,2-dibromo-3-nitrilopropionamide (DBNPA) enhanced by a 14-mer peptide

Di Wang[a], Mahmoud Ramadan[a], Sith Kumseranee[b], Suchada Punpruk[b], Tingyue Gu[a,*]

[a] Department of Chemical & Biomolecular Engineering, Institute for Corrosion and Multiphase Technology, Ohio University, Athens 45701, USA
[b] PTT Exploration and Production, Bangkok 10900, Thailand

ARTICLE INFO

Article history:
Received 5 February 2020
Received in revised form 29 February 2020
Accepted 29 February 2020
Available online 3 June 2020

Keywords:
Hydrotest
Microbiologically influenced corrosion
Anti-biofilm peptide
Biocide enhancer
2,2-dibromo-3-nitrilopropionamide (DBNPA)

ABSTRACT

In the oil and gas industry, microbiologically influenced corrosion (MIC) is a major threat to hydrotest, a procedure which is required to certify whether a pipeline can be commissioned. Seawater is frequently used as a hydrotest fluid. In this biofilm prevention lab study, an oilfield biofilm consortium was grown in an enriched artificial seawater anaerobically at 37 °C for 60 days. The combination of 100 ppm (w/w) 2,2-dibromo-3-nitrilopropionamide (DBNPA) + 100 nM (180 ppb) Peptide A (a biofilm dispersal agent) led to extra SRB (sulfate reducing bacteria), APB (acid producing bacteria) and GHB (general heterotrophic bacteria) sessile cell count reductions of 0.9-log, 0.8-log and 0.6-log, respectively, compared with the outcome obtained by using 100 ppm DBNPA only. The Peptide A enhancement also led to extra reductions of 44 % in weight loss, 43 % in maximum pit depth, and 54 % in corrosion current density.

1. Introduction

In the oil and gas industry, pipelines must be tested to ensure their mechanical integrity before transporting crude oil or gas over long distances. The general procedure used for this testing is known as pipeline hydrotest [1]. Seawater is frequently used in hydrotest [2,3]. In hydrotest, seawater is pressurized up to 125 % of the design maximum allowable operating pressure for a duration of 8–10 h to determine if there are any leaks [2–4]. Even though the actual pressure testing itself lasts just a few hours, the seawater in the pipeline is typically shut in as a parking liquid for weeks, months or up to one year until the pipeline is commissioned for service [2–4]. If organic carbon sources exist in the hydrotest seawater, they can support the growth of biofilms, which can cause microbiologically influenced corrosion (MIC) [5].

MIC is becoming a major area in metal corrosion research [6–13]. It is a threat in many industrial sectors [14,15]. MIC caused the failure of an 8″ oil transport pipeline in just 8 months [15]. MIC was likely the culprit for the Trans-Alaska Pipeline leak in the spring of 2006 [16]. Among numerous types of corrosive microorganisms, sulfate reducing bacteria (SRB) are the most reported corrosive microorganisms causing MIC in oilfields [17,18].

In addition to SRB and sulfate reducing archaea (SRA), acid producing bacteria (APB) and methanogens, other bacteria have also been identified in corrosive oilfield biofilms [19]. Extracellular electron transfer (EET) in EET-MIC between iron and corroding microbes requires biofilms because EET cannot be carried out across a body of fluid between planktonic cells and iron. Biofilms harbor more concentrated corrosive metabolites in MIC caused by metabolites (M-MIC) [20,21]. Thus, the mitigation of both types of MIC caused by microbes often means the mitigation of their biofilms.

Biocide treatment using oxidizing or non-oxidizing biocides, is a traditional method to control MIC in addition to physical scrubbing (or pigging) [22–24]. THPS (tetrakis hydroxymethyl phosphonium sulfate) and glutaraldehyde are the most prevalent biocides in oilfields because of their excellent efficacy and biodegradability [25,26]. Many chemicals have been tested for MIC mitigation. Some peptides have been found to possess antimicrobial abilities [27,28]. However, there are no large-scale industrial applications so far.

It has been repeatedly proven that sessile cells embedded in biofilms are far more resistant to antimicrobial treatment than free-floating planktonic cells in the bulk fluid [29]. If a biocide is used

* Corresponding author.
E-mail address: gu@ohio.edu (T. Gu).

https://doi.org/10.1016/j.jmst.2020.02.087
1005-0302/

for a long time for the same system, tougher microbes are enriched. New resistant microbes can move in to fill the vacancy left behind by less resistant microbes [30]. This causes biocide dosage escalation over time, which causes problems such as high operational cost and adverse environmental impact [31].

Researchers have utilized different biocide enhancers to make existing biocides more effective at the same or a reduced dosage [25]. Some enhancers are not biocidal at the tested low dosages, but they can enhance the efficacies of biocides in various ways [32]. Jia et al. reported that a 100 ppm D-amino acids mixtures combined with 60 ppm alkyldimethylbenzylammonium chloride (ADBAC) achieved SRB sessile cell count reduction by several logs compared to using ADBAC alone [33]. Two ppm D-tyrosine enhanced 30 ppm ciprofloxacin (CIP), leading to an extra 2-log nitrate-reducing *Pseudomonas aeruginosa* sessile cell count reduction vs. 30 ppm CIP only treatment [34]. Thus, D-amino acids are useful biocide enhancers because of their biofilm dispersal abilities [35,36]. More biocide enhancers are desired to combat problematic biocide enhancers.

Some organisms are able to maintain a biofilm-free exterior by secreting anti-biofilm agents. *Actinia equine*, a sea anemone, maintains a biofilm-free exterior by deploying Equinatoxin II protein. This protein has a 12-mer amino acid sequence of ser-val-pro-tyr-asp-tyr-asn-trp-tyr-ser-asn-trp that is highly conserved in several other organisms such as *Physcomitrella patens* (moss), *Danio rerio* (zebra fish) and *Tetraodon nigroviridis* (pufferfish), which also have biofilm-free exteriors [32]. This protein itself is not feasible as a biocide enhancer due to its unfavorable cost and stability. Peptide A was engineered with the 12-mer anti-biofilm sequence by adding L-cysteine at the two ends to make a cyclic 14-mer peptide (cys-ser-val-pro-tyr-asp-tyr-asn-trp-tyr-ser-asn-trp-cys), which emulates the loop structure for the 12-mer section in Equinatoxin II [32,37]. This peptide from biomimicry has recently been shown to be a non-biocidal green biocide enhancer for THPS at a very low concentration in 14-day biofilm prevention tests [32].

In this study, a corrosive oilfield biofilm consortium was adopted for 60-day lab tests because of its high corrosiveness [38]. 2,2-dibromo-3-nitrilopropionamide (DBNPA), a non-oxidizing fast-kill broad-spectrum environmentally friendly biocide, was used for this study. Peptide A was chosen as the biocide enhancer to enhance DBNPA for the first time. Different experimental methods, including microbiological assays, corrosion tests and electrochemical measurements were used to investigate MIC mitigation in a stimulated hydrotest seawater.

2. Experimental

2.1. Bacteria, metal coupons and chemicals

An oilfield biofilm consortium codenamed Consortium II was used for testing. The metagenomic data of Consortium II were reported in a previous study [39]. Enriched artificial seawater (EASW) was adopted for the growth of Consortium II. The composition of EASW was (g/L): NaCl 23.476, $MgCl_2$ 4.965, $NaHCO_3$ 0.192, Na_2SO_4 3.917, $CaCl_2{\cdot}2H_2O$ 1.469, $SrCl_2{\cdot}6H_2O$ 0.04, KCl 0.664, KBr 0.096, H_3BO_3 0.026, trisodium citrate ($Na_3C_6H_5O_7$) 0.5, yeast extract 1.0, sodium lactate ($NaC_3H_5O_3$) 3.5, $CaSO_4{\cdot}2H_2O$ 0.1, NH_4Cl 0.1, $MgSO_4{\cdot}7H_2O$ 0.71, $Fe(NH_4)_2(SO_4)_2{\cdot}6H_2O$ 1.37, K_2HPO_4 0.05. A 5 % (w/w) sodium hydroxide solution was used to adjust EASW's pH to 7.0 before autoclaving.

C1018 carbon steel bars were purchased from McMaster-Carr Supply Company (Elmhurst, IL, USA) and cut into rectangular coupons. Their elemental composition was (wt.%): 0.20 % C, 1.40 % Mn, 0.04 % P, 0.55 % Cu, 0.04 % Si, 0.012 % Ni and balance Fe. All surfaces were protected by a Teflon paint except an exposed top surface (1.2 cm × 1.0 cm). The coupons were abraded to a 600-grit finish before being cleaned using pure isopropanol and dried under UV light. After sterilization in an autoclave (Model MLS-3751 L, Panasonic, Osaka, Japan), EASW was deaerated using N_2 (filter-sterilized) for 1 h.

Sigma-Aldrich (St Louis, MO, USA) supplied DBNPA and Bachem AG (Bubendorf, Switzerland) custom synthesized Peptide A (100 % purity). Both were dissolved in deionized water and filtered-sterilized through a 0.22 μm disposal Stericup filter (Millipore, Bedford, MA, USA).

Before inoculation, 100 mL EASW medium (with or without treatment chemicals), 3 coupons were put into each 125 mL anaerobic vial in a N_2-filled glovebox. A concentrated L-cysteine stock solution was used to supply 100 ppm L-cysteine in EASW as oxygen scavenger. Consortium II seed culture to EASW volumetric ratio was 1:100 for inoculation. Anaerobic incubation at 37 °C lasted for 60 days in the biofilm prevention test.

2.2. Sessile cell counting and biofilm imaging

Three most probable number (MPN) liquid culture media were purchased from Biotechnology Solutions (Houston, TX, USA) for counting sessile SRB, APB and GHB (general heterotrophic bacteria) cells, respectively [39]. After the 60-day incubation at 37 °C, coupons were analyzed. The procedure of how to collect sessile cells for MPN assay is reported elsewhere [39]. For each sessile cell count data point, a total of three coupons from three replicate 125 mL vials were used for improved MPN accuracy [40].

2.3. Biofilm imaging

A scanning electron microscope (SEM) (Model JSM-6390, JEOL, Tokyo, Japan) was used. The coupon preparation method for biofilm SEM imaging was reported previously [33]. A confocal laser scanning microscope (CLSM) (Model LSM 510, Carl Zeiss, Jena, Germany) was used to distinguish live and dead sessile cells. Details on the sample preparations for CLSM are available elsewhere [33].

2.4. Weight loss and pitting corrosion analysis

In accordance with ASTM G1–03 [41], coupons were cleaned for 1 min using a fresh Clarke's solution followed by rinsing with anhydrous isopropanol and air drying before weighing on a balance and corrosion pit examination under SEM. The coupon surface after removing the biofilm and corrosion products was scanned under an infinite focus microscope (IFM) profilometer (Model ALC13, Alicona Imaging, Graz, Austria) and the pit depth profiles for different treatments were obtained. The maximum pit depths of six coupons from two replicate vials were used to give an (average) maximum pit depth data point.

Uniform corrosion rate was calculated from weight loss as shown below:

$$\mathrm{CR\,(mm/y)} = \frac{8.76\times10^4\times\Delta m}{\rho S t} \tag{1}$$

where CR is the uniform corrosion rate (mm/y), Δm the coupon weight loss (g), S the corroded surface area (cm^2), ρ the density of carbon steel (g/cm^3) and t the corrosion time (h).

Relative pitting severity (RPS) parameter was adopted to assess the relative severity of pitting corrosion (vs. uniform corrosion). It was calculated from Eq. (2) below [42].

$$\mathrm{RPS} = \frac{\text{Maximum pit growth rate (mm/y)}}{\mathrm{CR\,(mm/y)}} = \frac{\mathrm{Maximumpitdepth(cm)}\times\mathrm{metaldensity(mg/cm^3)}}{\text{weight loss (mg/cm}^2\text{)}} \tag{2}$$

If pitting corrosion is more severe than uniform corrosion, RPS is greater than unity. A near-unity RPS means that pitting corrosion and uniform corrosion are equally important. Because of different underlining corrosion mechanisms, the same biofilm can corrode different metals with very different RPS values. For example, *Desulfovibrio vulgaris* corroded copper and C1018 carbon steel with RPS values of 0.98 and 6.8, respectively in short-term tests, because the formal belongs to M-MIC, and the latter EET-MIC with pitting dominating [17,42].

2.5. Electrochemical measurements

In addition to weight loss and pit image analyses, a set of three-electrode glass cells were used for electrochemical measurements in this study. In each glass cell, the counter electrode was a thin platinum sheet, and reference electrode was a saturated calomel electrode (SCE). The working electrode was fabricated by embedding a C1018 carbon steel cube (exposed surface area 1.2 cm^2) in epoxy with connection to a sheathed copper wire. Three hundred mL EASW medium and 3.0 mL 3-day old Consortium II seed culture were added to each 450-mL glass cell. Different treatment chemicals were added to the glass cells upon inoculation. A PCI4/750 Potentiostat (Gamry Instruments, Warminster, PA, USA) with Gamry corrosion software (version 6.33) was used to perform linear polarization resistance (LPR) and potentiodynamic polarization (PDP) scans. The voltage range of LPR was −10 mV to 10 mV vs. the stabilized open circuit potential (OCP) at a scan rate of 0.167 mV/s. The voltage range was from −200 mV–200 mV vs. the OCP at a rate of 0.167 mV/s for PDP scans. LPR scans were performed daily while a PDP scan was done only at the end of the incubation period for each working electrode due to PDP's film-damaging wide voltage range.

3. Results and discussion

3.1. Sessile cell counts

The sessile cell counts after the 60-day incubation were shown in Fig. 1. The no treatment control coupon yielded cell counts of 2.1×10^7 cells/cm^2, 7.5×10^6 cells/cm^2, and 1.2×10^6 cells/cm^2 for sessile SRB, APB and GHB, respectively. There was no large difference in cell counts in respective SRB, GHB and APB categories with and without the treatment of 100 nM Peptide A only, which indicates that Peptide A alone at 100 nM was unable to inhibit the biofilm in the absence of a biocide stress. This was because the biofilm was a recalcitrant mixed-culture oilfield biofilm [43]. With the treatment of 100 ppm DBNPA only, there were 1.3-log, 1.4-log and 0.4-log reductions in SRB, GHB and APB sessile cell counts, respectively. With the combination of 100 ppm DBNPA + 100 nM Peptide A, there were additional 0.9-log, 0.8-log and 0.6-log reductions compared to the 100 ppm DBNPA only treatment. The additional sessile cell count reductions demonstrated the enhancement effect of Peptide A for 100 ppm DBNPA in the prevention of the biofilm establishment on carbon steel.

3.2. Biofilm observation

CLSM was used to visualize biofilms on coupons. Fig. 2 shows that the no treatment control coupon and the 100 nM Peptide A only treatment coupon both had very good biofilm coverages. In the presence of 100 ppm DBNPA, lots of sessile cells were killed (red dots in Fig. 2(C)), but a few sessile cells survived (green dots in Fig. 2(C)). When enhanced by 100 nM (180 ppb) Peptide A, 100 ppm DBNPA killed more sessile cells and less biofilm biomass was left on the coupon surface. The reduction in the biofilm biomass was partially caused by the biofilm disposal effect of Peptide A in

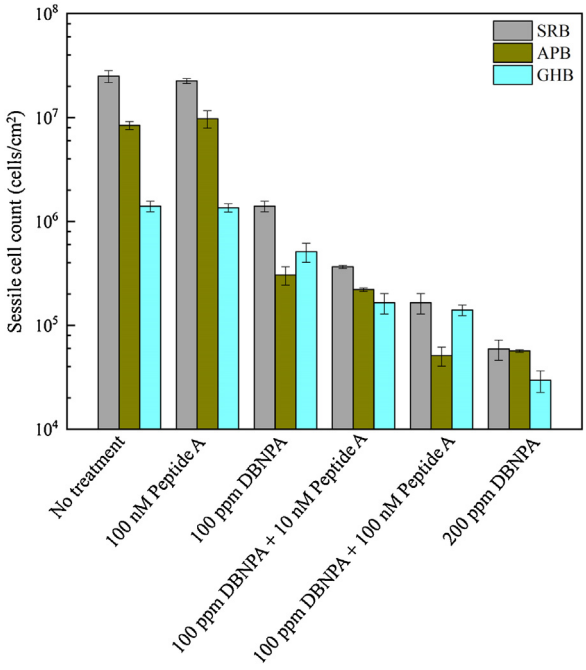

Fig. 1. Sessile cell counts of SRB, GHB and APB on C1018 coupons after 60 days. (Each sessile cell count data point represents the average of 3 readings, each from a coupon in a replicate run.).

view that almost all sessile cells were dead with the treatment of 200 ppm DBNPA, but there was more biofilm biomass remaining on the coupon surface (Fig. 2(F)). Thus, the high dosage DBNPA killed more cells but dead cells stayed on the biofilm because they died recently and were not decomposed yet. The comparison of Fig. 2(E) vs. Fig. 2(F) suggests a biofilm dispersal effect by Peptide A in the presence of a biocide stress (i.e., 100 ppm DBNPA + 100 nM Peptide A treatment).

Surface morphologies of biofilms are shown in Fig. 3. Abundant live sessile cells are seen on the no treatment control coupon and 100 nM Peptide A only treatment coupon in Fig. 3(A) and (B). With the 100 ppm DBNPA only treatment and the combination treatment of 100 ppm DBNPA + 10 nM Peptide A, fewer live sessile cells were present, but some live sessile cells were still there. With 100 ppm DBNPA + 100 nM Peptide A (Fig. 3(E)), there were much less live sessile cells than with the 100 ppm DBNPA only treatment. Fig. 3(E) shows that the 100 ppm DBNPA + 100 nM Peptide A treatment appeared to be comparable to the 200 ppm DBNPA treatment (Fig. 3(F)). The parallel polishing lines on the base metal are visible on coupon surfaces in Fig. 3(E) and (F). The biofilm morphologies here corroborated sessile cell count results.

3.3. Corrosion analyses

Corrosion pits were obvious on the no treatment control (Fig. 4(A)) and the 100 nM Peptide A only (Fig. 4(B)) coupons. The 100 ppm DBNPA only treatment and the 100 ppm DBNPA + 10 nM Peptide A treatment (Fig. 4(C) and 4(D)) led to smaller and fewer pits. For the 100 ppm DBNPA + 100 nM Peptide A treatment, fewer pits can be seen in Fig. 4(E) and the coupon polishing lines are visible. Fig. 4(E) and 4(F) suggest that 100 ppm DBNPA + 100 nM Peptide A were comparable in corrosion mitigation outcome to 200 ppm DBNPA.

Corrosion weight loss data are shown in Fig. 5. The weight loss was 15.7 mg/cm^2 (equivalent to 0.12 mm/y uniform corrosion rate) for the no treatment control. For 100 nM Peptide A only treatment, the weight loss was 13.3 mg/cm^2 (0.10 mm/y), indicating that 100

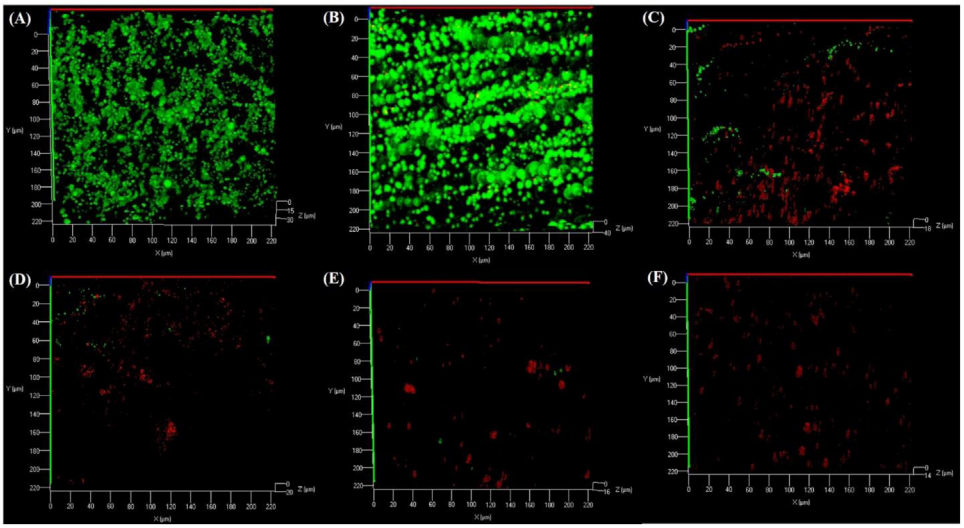

Fig. 2. CLSM biofilm images (live cells green and dead cells red) on carbon steel coupons after 60 days: (A) no treatment, (B) 100 nM Peptide A, (C) 100 ppm DBNPA, (D) 100 ppm DBNPA + 10 nM Peptide A, (E) 100 ppm DBNPA + 100 nM Peptide A, and (F) 200 ppm DBNPA.

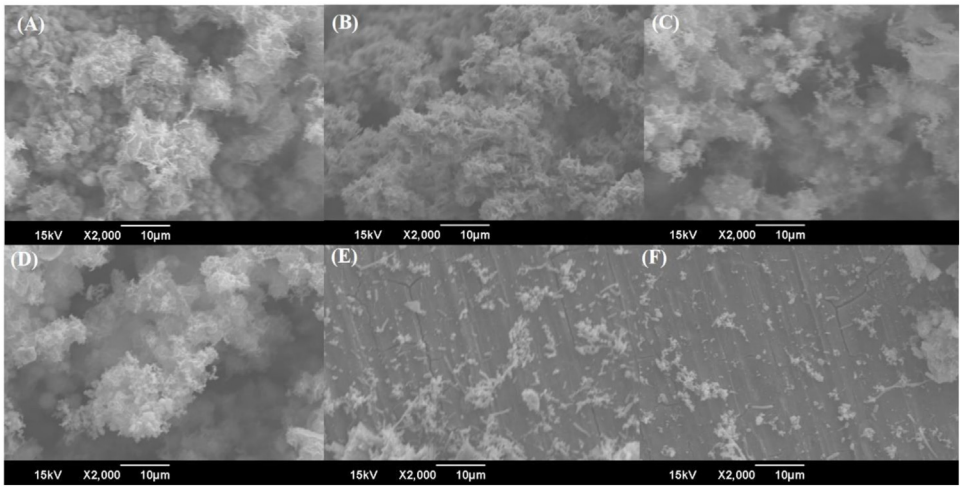

Fig. 3. SEM biofilm images on carbon steel coupons after 60 days: (A) no treatment, (B) 100 nM Peptide A, (C) 100 ppm DBNPA, (D) 100 ppm DBNPA + 10 nM Peptide A, (E) 100 ppm DBNPA + 100 nM Peptide A, and (F) 200 ppm DBNPA.

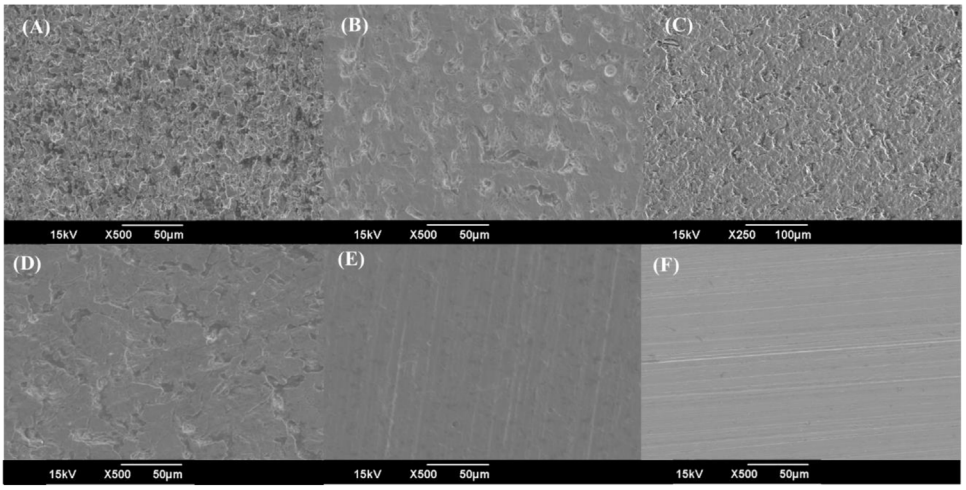

Fig. 4. SEM corroison pit images on carbon steel coupons after 60 days: (A) no treatment, (B) 100 nM Peptide A, (C) 100 ppm DBNPA, (D) 100 ppm DBNPA + 10 nM Peptide A, (E) 100 ppm DBNPA + 100 nM Peptide A, and (F) 200 ppm DBNPA.

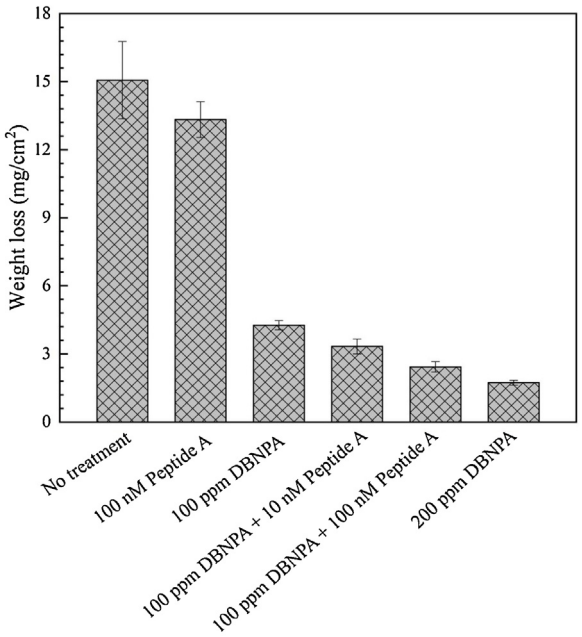

Fig. 5. Weight losses of coupons with different treatments after 60 days. (Each scatter band is the standard deviation of 3 independent samples).

nM Peptide A had only very little effect on the weight loss. This was expected for a tough biofilm. With the treatment of 100 ppm DBNPA only, the weight loss was reduced greatly to 4.3 mg/cm^2 (0.033 mm/y). The combination of 100 ppm DBNPA + 100 nM Peptide A treatment further reduced the weight loss by 44 % to 2.4 mg/cm^2 (0.019 mm/y), which was not very far from the 1.7 mg/cm^2 weight loss (0.013 mm/y) achieved by the 200 ppm DBNPA only treatment. Figs. 3 and 5 proved that a treated weaker biofilm led to less corrosion.

Fig. 6 shows the IFM pit depth profiles on C1018 carbon steel coupons after the 60-day incubation with different biocide treatments. The maximum pit depth reached 73.4 μm after 60 days without treatment. With the 100 nM Peptide A only treatment, it decreased slightly to 61.9 μm. It dropped steeply to 19.7 μm in the presence of 100 ppm DBNPA. It dropped further by 43 % to 11.2 μm for the 100 ppm DBNPA + 100 nM Peptide A treatment. The maximum pit depth was the lowest at 9.7 μm for the 200 ppm DBNPA treatment. For all the test conditions in this work, the RPS values for C1018 carbon steel fell into a very narrow range of 3.5–3.7. Thus, RPS was a reliable parameter to use weight loss data to predict pit depths using Eq. (2) in this work. The average RPS value of 3.6 here is smaller than the 6.8 obtained for *D. vulgaris* in ATCC 1249 culture medium after 7 days of incubation because this work used a different biofilm in a different culture medium for a much longer incubation time. The value of 3.6 is still much larger than unity, indicating that pitting was more important than uniform corrosion.

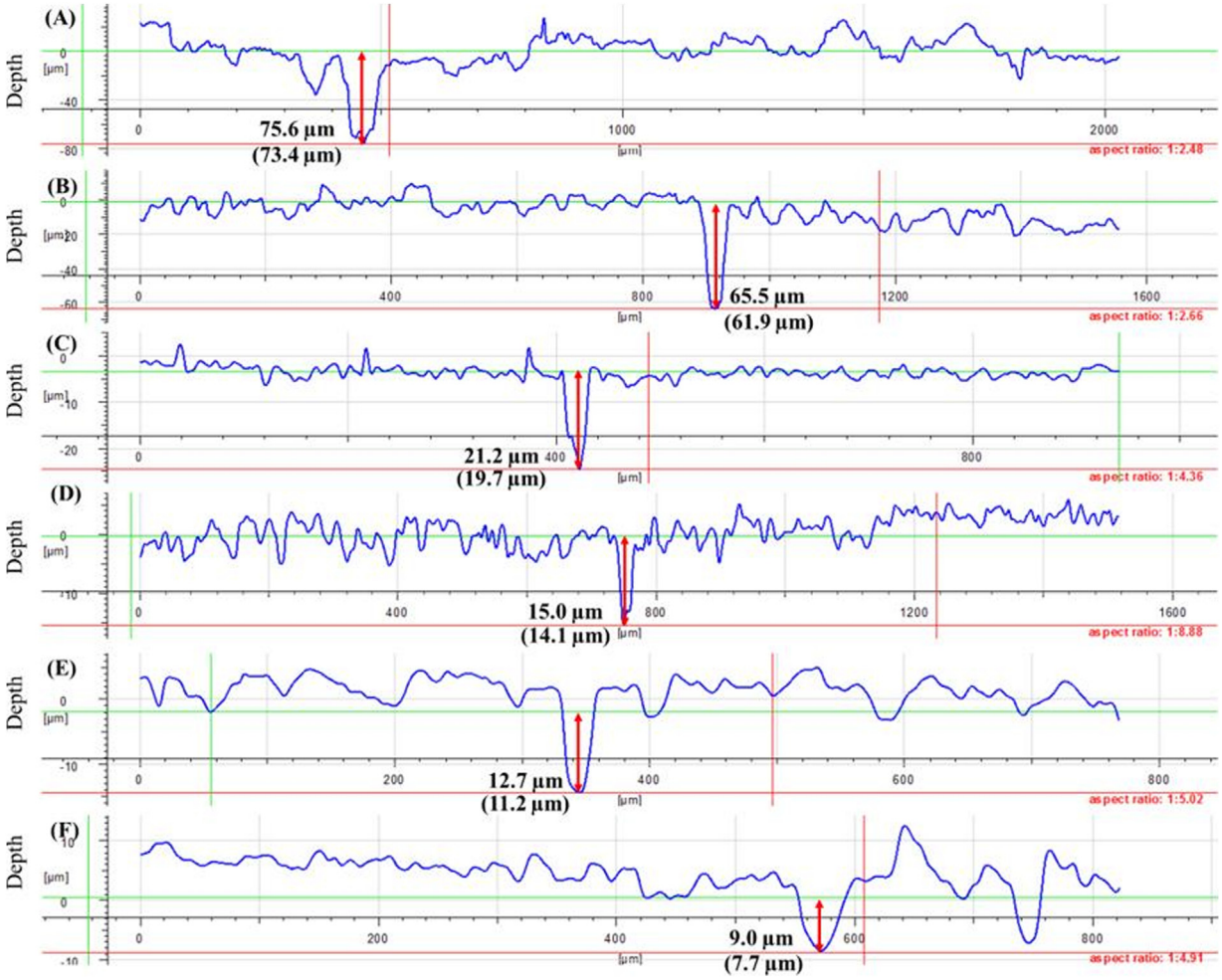

Fig. 6. A representative set of IFM pit depth profiles of coupons after 60 days (average values in brackets from 6 coupons): (A) no treatment, (B) 100 nM Peptide A, (C) 100 ppm DBNPA, (D) 100 ppm DBNPA + 10 nM Peptide A, (E) 100 ppm DBNPA + 100 nM Peptide A, and (F) 200 ppm DBNPA.

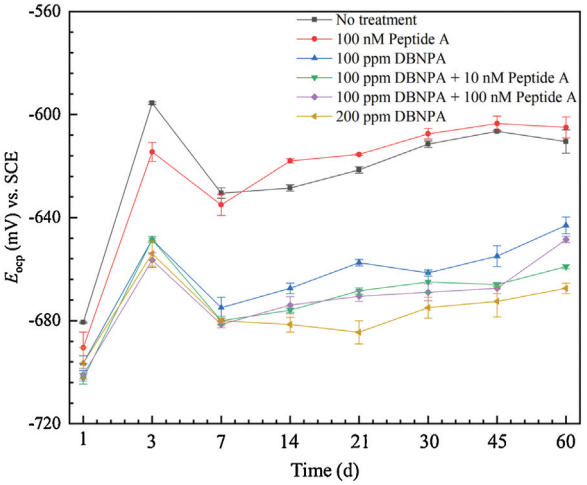

Fig. 7. Variations of OCP for different biocide treatments.

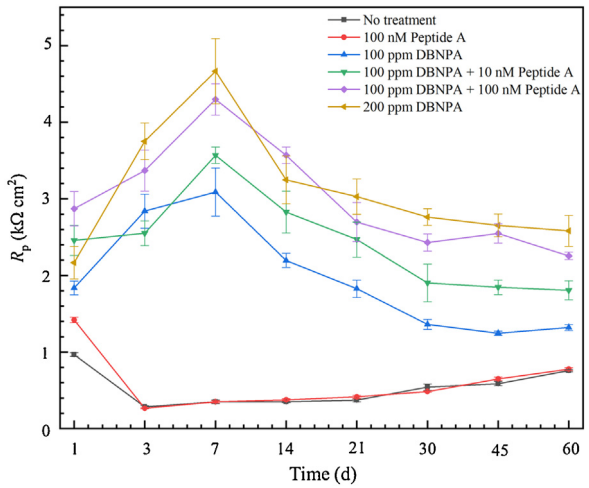

Fig. 8. Variations of polarization resistance (R_p) for different treatments.

3.4. Electrochemical measurements

Electrochemical tests can provide transient corrosion behavior unlike cumulative weight loss and pitting data. OCP vs. time curves are shown in Fig. 7. All the OCP values were not too far from each other on the first day. They moved higher during the initial 3 days and started to decline until the 7th day. The OCP values were higher with no treatment and for the 100 nM Peptide A only treatment than those with the DBNPA only treatment and the DBNPA + Peptide A treatment. All the values increased only slightly from the 7th day to the end of the 60-day incubation period.

A lower OCP suggests a higher thermodynamic tendency for the working electrode to lose electrons (i.e., to be corroded). However, corrosion outcome is determined not only by thermodynamic driving force, but also by kinetic parameters such as the exchange current density for charge transfer as shown in the Butler-Volmer equation [44]. In a complicated culture medium with many nutrients and metabolites, an oxidant may cause a very negative OCP, i.e., a very strong thermodynamic tendency for it to take electrons from the working electrode, when the actual corrosion rate is not being measured (i.e., at OCP condition). However, the corrosion kinetic process for the oxidant to corrode can be insignificant due to a large activation energy for its reduction. Thus, it is not surprising to see the unusual OCP trend in Fig. 7 showing a more effective biocide treatment yielding a lower OCP (i.e., a higher thermodynamic tendency for corrosion) rather than a higher OCP. This kind of misleading OCP behavior was reported in SRB MIC of carbon steel cases. In the same MIC cases, corrosion kinetic data were found to be meaningful and consistent with weight loss and pitting data [17,45]. Thus, it can be erroneous using OCP thermodynamic data to predict actual corrosion trends without verification by kinetic electrochemical measurements in complicated MIC systems.

Fig. 8 shows the polarization resistance (R_p) time course data for different biocide treatments. A higher R_p means less corrosion. The R_p values were very close for the no treatment control and the 100 nM Peptide A only treatments. This indicates that the 100 nM Peptide A only treatment did not inhibit corrosion. In Fig. 8, 100 ppm DBNPA's R_p curve is much higher than that for the no treatment control, which means good corrosion inhibition with the biocide treatment. When 10 nM Peptide A was used to enhance 100 ppm DBNPA, its R_p curve moved higher. The R_p curve was further elevated when 100 nM Peptide A was used instead of 10 nM Peptide to enhance 100 ppm DBNPA. The largely overlapping R_p curves for the 200 ppm DBNPA only treatment and the 100 ppm DBNPA + 100 nM Peptide A treatment in Fig. 8 suggest that they were comparable in corrosion inhibition with the former slighter better.

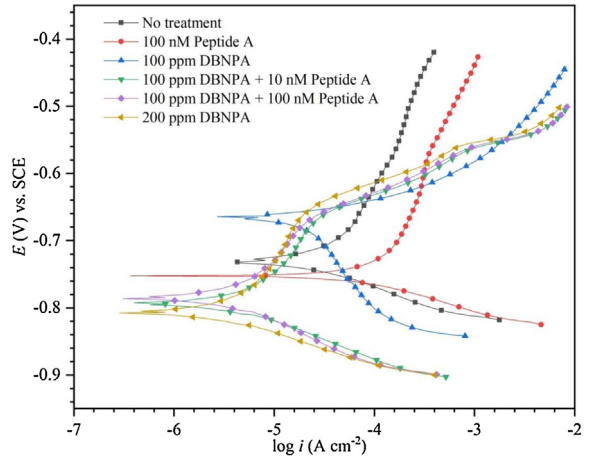

Fig. 9. Potentiodynamic polarization plots obtained at the end of the 60-day of incubation.

Fig. 9 shows the PDP scans for all treatments at the end of the biofilm prevention test in the electrochemical glass cells. The corresponding Tafel parameters are listed in Table 1. The corrosion current density i_{corr} values for the no treatment control and the 100 nM Peptide A only treatment were 43.2 μA/cm^2 and 46.2 μA/cm^2, respectively, which were much larger than that of the 100 ppm DBNPA only treatment (11.9 μA/cm^2). The i_{corr} values of 10 nM Peptide A + 100 ppm DBNPA (7.1 μA/cm^2) and 100 ppm DBNPA + 100 nM Peptide A (5.5 μA/cm^2) were lower when compared with the 100 ppm DBNPA only treatment, indicating improved efficacy. Compared to the 100 ppm DBNPA only treatment, there was an additional 54 % reduction in i_{corr} with the enhancement of 100 nM Peptide A. The i_{corr} value of 100 ppm DBNPA + 100 nM Peptide A was only slightly larger than that for 200 ppm DBNPA (5.5 μA/cm^2 vs. 4.7 μA/cm^2). The i_{corr} data and LPR data here corroborate the weight loss data above. These data suggest that electrochemical measurements, excluding OCP thermodynamic tendency data, are reliable tools in assessing biocide efficacy. Note that the i_{corr} data reflected only the corrosion at the end of the incubation period while the R_p data were transient data. R_p data should be used to predict corrosion trends, but not for calculating corrosion rates because Tafel slopes vary greatly for different test conditions and for different times in complicated MIC systems.

Table 1
Electrochemical parameters from Tafel analysis of PDP scans at the end of the 60-day incubation.

	i_{corr} (μA/cm^2)	E_{corr} (mV) vs. SCE	β_a (mV/dec)	β_c (mV/dec)
No treatment	43.2	−732	300	71
100 nM Peptide A	46.2	−752	421	63
100 ppm DBNPA	11.9	−667	30	40
100 ppm DBNPA + 10 nM Peptide A	7.1	−794	22	76
100 ppm DBNPA + 100 nM Peptide A	5.5	−785	180	86
200 ppm DBNPA	4.7	−804	224	64

4. Conclusion

After 60 days of incubation at 37 °C in the simulated hydrotest test fluid, the 75.6 μm maximum pit depth and 15.7 mg/cm^2 weight loss (0.12 mm/y) indicate a potentially serious MIC problem in hydrotest caused by the oilfield biofilm Consortium II. The Peptide A only treatment had a negligible impact on the recalcitrant biofilm consortium. However, the combination of 100 ppm DBNPA + 100 nM Peptide A had a good efficacy on the inhibitation of bacterial growth and corrosion reduction compared to the 100 ppm DBNPA only treatment. The enhancement by Peptide A led to 44 % further reduction in weight loss and 43 % further reduction in maximum pit depth. Relative pitting severity RPS values were found to fall into a very narrow range of 3.5–3.7 for the test conditions in this work, making RPS useful to predict maximum pit depth from weight loss or vice versa. Weight loss, maximum pit depth, biofilm coverage and electrochemical results showed consistent corrosion trends. It was shown that kinetic electrochemical results were useful in assessing biocide efficacy in this work, while OCP data were misleading in this complicated SRB system.

Acknowledgement

This work was financially supported by PTT Exploration and Production, Thailand and Chinese Society for Corrosion and Protection.

References

[1] M.S. Keys, US Patent 5197324 (1993).
[2] T. Unsal, R. Jia, S. Kumseranee, S. Punpruk, T. Gu, Eng. Failure Anal. 100 (2019) 544–555.
[3] D. Xu, W. Huang, G. Ruschau, J. Hornemann, J. Wen, T. Gu, Eng. Failure Anal. 28 (2013) 149–159.
[4] L. Machuca Suarez, in: Proceedings to Annual Conference of the Australasian Corrosion Association 2014, Corrosion and Prevention 2014, Darwin, Austrilia, 2014, pp. 21–24, September.
[5] R. Jia, D. Wang, P. Jin, T. Unsal, D. Yang, J. Yang, D. Xu, T. Gu, Corros. Sci. 153 (2019) 127–137.
[6] D. Xu, E. Zhou, Y. Zhao, H. Li, Z. Liu, D. Zhang, C. Yang, H. Lin, X. Li, K. Yang, J. Mater. Sci. Technol. 34 (2018) 1325–1336.
[7] D. Liu, R. Jia, D. Xu, H. Yang, Y. Zhao, M. saleem Khan, S. Huang, J. Wen, K. Yang, T. Gu, J. Mater. Sci. Technol. 35 (2019) 2494–2502.
[8] H. Li, C. Yang, E. Zhou, C. Yang, H. Feng, Z. Jiang, D. Xu, T. Gu, K. Yang, J. Mater. Sci. Technol. 33 (2017) 1596–1603.
[9] E. Zhou, D. Qiao, Y. Yang, D. Xu, Y. Lu, J. Wang, J.A. Smith, H. Li, H. Zhao, P.K. Liaw, F. Wang, J. Mater. Sci. Technol. 46 (2020) 201–210.
[10] Y. Dong, Y. Lekbach, Z. Li, D. Xu, S. El Abed, S. Ibnsouda Koraichi, F. Wang, J. Mater. Sci. Technol. 37 (2020) 200–206.
[11] T. Gu, R. Jia, T. Unsal, D. Xu, J. Mater. Sci. Technol. 35 (2019) 631–636.
[12] Y. Li, D. Xu, C. Chen, X. Li, R. Jia, D. Zhang, W. Sand, F. Wang, T. Gu, J. Mater. Sci. Technol. 34 (2018) 1713–1718.
[13] W. Dou, J. Liu, W. Cai, D. Wang, R. Jia, S. Chen, T. Gu, Corros. Sci. 150 (2019) 258–267.
[14] C.N. Street, A. Gibbs, Corros. Sci. 52 (2010) 1447–1452.
[15] S. Bhat, B. Kumar, S. Prasad, M. Katarki, Mater. Perform. 50 (2011) 50–54.
[16] G.A. Jacobson, Mater. Perform. 46 (2007) 26–35.
[17] R. Jia, J.L. Tan, P. Jin, D.J. Blackwood, D. Xu, T. Gu, Corros. Sci. 130 (2018) 1–11.
[18] H. Liu, T. Gu, G. Zhang, H. Liu, Y.F. Cheng, Corros. Sci. 136 (2018) 47–59.
[19] E.J. Summer, S. Duggleby, C. Janes, M. Liu, in: Proceedings to Corrosion, Paper No. 2014-4376, NACE International, San Antonio, Texas, USA, 2014.
[20] R. Jia, T. Unsal, D. Xu, Y. Lekbach, T. Gu, Int. Biodeterior. Biodegrad. 137 (2019) 42–58.
[21] D.J. Beale, P.D. Morrison, C. Key, E.A. Palombo, Water Sci. Technol. 69 (2013) 1–8.
[22] S. Shakeri, R.K. Kermanshahi, M.M. Moghaddam, G. Emtiazi, Biofouling 23 (2007) 79–86.
[23] J. Wang, T. Zhang, X. Zhang, M. Asif, L. Jiang, S. Dong, T. Gu, H. Liu, J. Mater. Sci. Technol. 43 (2020) 14–20.
[24] J. Xu, R. Jia, D. Yang, C. Sun, T. Gu, J. Mater. Sci. Technol. 35 (2019) 109–117.
[25] D. Xu, R. Jia, Y. Li, T. Gu, World J. Microbiol. Biotechnol. 33 (2017) 97.
[26] M. Sharma, H. Liu, S. Chen, F. Cheng, G. Voordouw, L. Gieg, Sci. Rep. 8 (2018) 1–12.
[27] G. Laverty, S.P. Gorman, B.F. Gilmore, Int. J. Mol. Sci. 12 (2011) 6566–6596.
[28] A.A. Bahar, D. Ren, Pharmaceuticals 6 (2013) 1543–1575.
[29] M.J. Franklin, D.E. Nivens, A.A. Vass, M.W. Mittelman, R.F. Jack, N.J.E. Dowling, D.C. White, Corrosion 47 (1991) 128–134.
[30] P.A. Rasheed, K.A. Jabbar, K. Rasool, R.P. Pandey, M.H. Sliem, M. Helal, A. Samara, A.M. Abdullah, K.A. Mahmoud, Corros. Sci. 148 (2019) 397–406.
[31] R. Zuo, Appl. Microbiol. Biotechnol. 76 (2007) 1245–1253.
[32] R. Jia, D. Yang, W. Dou, J. Liu, A. Zlotkin, S. Kumseranee, S. Punpruk, X. Li, T. Gu, Int. Biodeterior. Biodegrad. 139 (2019) 78–85.
[33] R. Jia, D. Yang, Y. Li, D. Xu, T. Gu, Int. Biodeterior. Biodegrad. 117 (2017) 97–104.
[34] R. Jia, D. Yang, D. Xu, T. Gu, Sci. Rep. 7 (2017) 6946.
[35] I. Kolodkin-Gal, D. Romero, S. Cao, J. Clardy, R. Kolter, R. Losick, Science 328 (2010) 627–629.
[36] D. Romero, R. Kolter, Trends Microbiol. 19 (2011) 304–306.
[37] A. Zlotkin, US Patent 9284351 (2016) B2.
[38] R. Jia, Y. Li, H.H. Al-Mahamedh, T. Gu, Front. Microbiol. 8 (2017) 1538.
[39] R. Jia, D. Yang, H.H. Al-Mahamedh, T. Gu, Ind. Eng. Chem. Res. 56 (2017) 7640–7649.
[40] S. Sutton, J. Valid. Technol. 16 (2010) 35–38.
[41] ASTM G1-03, Standard Practice for Preparing, Cleaning, and Evaluating Corrosion Test Specimens, 2003.
[42] W. Dou, R. Jia, P. Jin, J. Liu, S. Chen, T. Gu, Corros. Sci. 144 (2018) 237–248.
[43] Y. Li, R. Jia, H.H. Al-Mahamedh, D. Xu, T. Gu, Front. Microbiol. 7 (2016) 896.
[44] D. Xu, Y. Li, T. Gu, Bioelectrochemistry 110 (2016) 52–58.
[45] H. Liu, C. Fu, T. Gu, G. Zhang, Y. Lv, H. Wang, H. Liu, Corros. Sci. 100 (2015) 484–495.